Multimodel Evidence of Future Tropical Atlantic Precipitation Change Modulated by AMOC Decline

Multimodel Evidence of Future Tropical Atlantic Precipitation Change Modulated by AMOC Decline

GIADA CERATO,[a] KATINKA BELLOMO,[a,b] ROBERTA D'AGOSTINO,[c] AND JOST VON HARDENBERG[a,b]

[a] *Department of Environment, Land, and Infrastructure Engineering, Politecnico di Torino, Turin, Italy*
[b] *National Research Council, Institute of Atmospheric Sciences and Climate, Turin, Italy*
[c] *National Research Council, Institute of Atmospheric Sciences and Climate, Lecce, Italy*

(Manuscript received 17 June 2024, in final form 22 January 2025, accepted 3 February 2025)

ABSTRACT: Projections from global climate models reveal a significant intermodel spread in future rainfall changes in the tropical Atlantic by the end of the twenty-first century, including alterations to the intertropical convergence zone (ITCZ) and monsoonal regions. While existing studies have identified various sources of uncertainty, our research uncovers a prominent role played by the decline of the Atlantic meridional overturning circulation (AMOC) for the intermodel spread. First, we examine 30 climate model simulations (using the shared socioeconomic pathway (SSP) 5–8.5 scenario) from the CMIP6 archive and show that models that present a more substantial AMOC decline exhibit an equatorward shift of the ascending branch of the Atlantic regional Hadley circulation, resulting in a southward displacement of the ITCZ. Conversely, models characterized by a smaller AMOC decline do not indicate any ITCZ displacement. Second, we use targeted experiments (using the abrupt $4xCO_2$ experiment) to specifically isolate the effects of a weakened AMOC from the changes in precipitation that would occur if, under continuous global warming, the AMOC did not weaken. Our results demonstrate that net precipitation anomalies in the abrupt $4xCO_2$ experiments are displaced southward compared to the simulation with fixed AMOC strength, corroborating our previous findings. Our study has implications for understanding the mechanisms driving future changes in tropical Atlantic precipitation and underscores the central role played by the AMOC in future climate change.

KEYWORDS: Atlantic Ocean; Intertropical convergence zone; Atmosphere-ocean interaction; Climate change

1. Introduction

The intertropical convergence zone (ITCZ) is a planetary-scale zonal band of intense precipitation activity. Typically, the ITCZ is located about 5°N of the equator in the annual mean (Philander et al. 1996). However, its location undergoes migration in response to solar insolation and interhemispheric energy imbalance (Broccoli et al. 2006; Chiang and Friedman 2012; Bischoff and Schneider 2014). Modifications in the strength, width, and seasonal displacements of the ITCZ can have far-reaching impacts, including severe droughts or extensive flooding, with significant implications for local communities (Fernandes et al. 2011; Marengo et al. 2012; Chiang et al. 2002). Atmospheric reanalyses and observations indicate recent intensification and narrowing of the ITCZ. For the coming years, idealized climate model simulations of future climate change generally project further narrowing and weakening of the mean ascent (Byrne et al. 2018; Mamalakis et al. 2021; Byrne and Schneider 2016). Nonetheless, previous studies have revealed significant intermodel uncertainty in simulating the response of tropical precipitation to future climate change. For instance, Byrne et al. (2018) demonstrated intermodel uncertainty in the meridional shift of the ITCZ in a warming climate using models from phase 5 of the Coupled Model Intercomparison Project (CMIP5) (Taylor et al. 2012), while Mamalakis et al. (2021) found that the intermodel spread persists in CMIP6 models (Eyring et al. 2016; O'Neill et al. 2016).

Previous research has established that the meridional position of the ITCZ in the mean climate is influenced by the interhemispheric energy transport (Donohoe et al. 2013; Donohoe 2016; Donohoe and Voigt 2017). Given its influence on cross-equatorial heat transport, the Atlantic meridional overturning circulation (AMOC) is thus believed to play a pivotal role in governing the ITCZ's position and meridional displacements (Frierson et al. 2013; Marshall et al. 2014; Schneider et al. 2014; Yu and Pritchard 2019; Moreno-Chamarro et al. 2020). In fact, in the mean climate, the AMOC transports ~0.5 PW of heat into the Northern Hemisphere (Buckley and Marshall 2016). In addition, several prior studies have employed climate models to conduct ad hoc experiments to investigate the impacts of reduced energy transport by the AMOC on precipitation. These studies demonstrated that a weakened AMOC results in reduced precipitation over the North Atlantic and a southward shift of the ITCZ's zonal-mean position over the tropical ocean (e.g., Vellinga and Wood 2002; Zhang and Delworth 2005; Stouffer et al. 2006; Parsons et al. 2014; Jackson et al. 2015; Good et al. 2022; Orihuela-Pinto et al. 2022). A southward shift of the ITCZ balances the reduced northward heat transport by the AMOC and is associated with

Denotes content that is immediately available upon publication as open access.

Supplemental information related to this paper is available at the Journals Online website: https://doi.org/10.1175/JCLI-D-24-0333.s1.

Corresponding author: Giada Cerato, giada.cerato@polito.it

DOI: 10.1175/JCLI-D-24-0333.1

a meridional displacement of the Hadley cells and an intensification of the ascending branch of the Northern Hemisphere Hadley cell (Zhang and Delworth 2005; Bellomo et al. 2023; Lionello et al. 2024). Consequently, the response of the AMOC to climate change might significantly impact the tropical Atlantic ITCZ in future climate scenarios, considering the general consensus among climate models on a substantial weakening of the AMOC by the twenty-first century (Weijer et al. 2020; Rahmstorf et al. 2015; Caesar et al. 2018; Bellomo et al. 2021). In particular, Bellomo et al. (2021) investigated abrupt 4xCO_2 simulations from the CMIP5 and CMIP6 archives and demonstrated that a sufficiently strong decline in the AMOC intensity can modulate the global precipitation response. Furthermore, idealized experiments with one global climate model showed that a weakened AMOC, relative to rising greenhouse gases, can lead to a southward shift of the tropical Atlantic ITCZ in the annual mean (Liu et al. 2020; Bellomo and Mehling 2024).

The specific role that the representation of the AMOC plays in the large intermodel spread in Atlantic ITCZ projections of the current century has remained largely unexplored, despite the potential significance of the AMOC's response to increasing greenhouse gases (Wang et al. 2014). In this study, we address this gap by employing a set of 30 latest-generation global climate models to examine the SSP5–8.5 high-emission scenario, where the AMOC undergoes substantial weakening by 2100, though the extent of its weakening is uncertain across models. Through this multimodel approach, we group models based on the magnitude of the AMOC decline, revealing that the spread in the representation of the AMOC decline is tightly linked to intermodel differences in anticipated changes of both tropical rainfall and mean atmospheric circulation over the Atlantic sector. Nevertheless, in these simulations, it is challenging to isolate the precipitation response due to the AMOC decline from that due to other climate feedbacks related to anthropogenic forcing and ongoing climate change. Therefore, to build consistency on our findings, we supplement our analysis with idealized model experiments using EC-Earth3, a global climate model that participates in CMIP6.

2. Materials and methods

a. Model simulations

We examine the annual-mean tropical Atlantic rainfall response to the AMOC decline in an ensemble of 30 model simulations from the CMIP6 archive (Eyring et al. 2016). We compare the SSP5–8.5 experiment with the historical run. The historical experiment was forced with observed estimates of human-induced and natural radiative forcings from 1850 to 2014 (O'Neill et al. 2016). The SSP5–8.5 future projection spans the years between 2015 and 2100 and was forced with estimates of greenhouse gas concentrations assuming a high emission scenario reaching a radiative forcing at the top of the atmosphere of 8.5 W m^{-2} by the end of the twenty-first century. The SSP5–8.5 experiment was initialized from the last year of the historical experiment. We analyze all 30 models that made available the variables needed for this study. Where available, we pick the r1i1p1f1 ensemble member. The list of models and the relative ensemble member is provided in Table 1.

In addition to the SSP5–8.5 simulations, we analyze two experiments carried out with the global climate model EC-Earth3. These experiments were started from the preindustrial control ("piControl") experiment (ensemble member r1i1p1f1) from the CMIP6 archive. The piControl experiment spans 500 years during which all the external radiative forcings are maintained at preindustrial levels (CO_2 at ~284 ppm). In the first experiment, the CO_2 was abruptly quadrupled from the mean annual preindustrial level and was held fixed for 150 years ("abrupt 4xCO_2") (Eyring et al. 2016). This experiment is stored in the CMIP6 archive (ensemble member r81i1p1f1). The second one is an ad hoc experiment that aims at maintaining the AMOC strength fixed at the preindustrial level, despite an abrupt fourfold increase in atmospheric CO_2 applied as external forcing. This was achieved by adding a virtual salinity flux poleward of 50°N in the North Atlantic and Arctic Oceans. We ran a small ensemble of three members for the second experiment. Although the three members share the same configuration as the EC-Earth3 version used in CMIP6 and initial conditions, they were forced with salinity fluxes of slightly different magnitudes [+0.4, +0.5, and +0.6 Sv (1 Sv $\equiv 10^6$ m^3 s^{-1})] to span the model's internal variability of AMOC strength in the preindustrial simulation (Meccia et al. 2023). We analyzed each member individually and found no large differences among them. Therefore, only results from the ensemble mean of the three members are presented, hereafter, referred to as the "PI-fixed AMOC" experiment. The abrupt 4xCO_2 and PI-fixed AMOC experiments allow us to separate the response of tropical rainfall to CO_2 forcing from the response to an AMOC weakening due to the same forcing, thereby isolating the impacts of the AMOC weakening on tropical rainfall. Note that these experiments are identical to those shown in Bellomo and Mehling (2024), and we refer the reader to that publication for further technical details. Time series of AMOC strength in the SSP5–8.5 and EC-Earth3 idealized experiments are shown in Fig. 1.

b. Data analysis and statistical methods

For the 30 SSP5–8.5 simulations, we define the control climatology as the time mean from the whole historical simulations (165 years spanning from 1850 to 2014). For each model, we compute changes as the difference between the mean of years from 2071 through 2100 (30 yr) of the SSP5–8.5 simulation and the control climatology. To ensure changes do not lie within the natural climate variability, we perform the Student's t test between the historical and the future time series, using a significance level of 90%. All models' output is interpolated to a common 2.5° × 2.5° latitude/longitude grid before performing the analysis.

To assess the impacts of the AMOC decline in the CMIP6 SSP5–8.5 scenario, relative to other changes, we create two groups of 10 models each (out of the 30 models employed in this study), based on the amount of the AMOC decline with respect to the control climatology (see Table 1). The models belonging to the group in which the AMOC declines less are

TABLE 1. List of models: model's name, variant label (ensemble member), AMOC change (in Sv and %) between the SSP5–8.5 simulations and the control climatology, AMOC historical mean strength, ΔGMTAS, and belonging group. The AMOC strength is calculated at 45°N.

Model name	Variant label	AMOC mean strength (Sv)	ΔAMOC (%)	ΔAMOC (Sv)	ΔGMTAS (°C)	Assigned group
INM-CM4-8	r1i1p1f1	7.73	−11.31	−0.87	3.32	SAD
INM-CM5-0	r1i1p1f1	8.65	−18.20	−1.57	3.17	SAD
CAS-ESM2-0	r1i1p1f1	15.92	−23.72	−3.78	4.45	SAD
MPI-ESM1-2-HR	r1i1p1f1	16.85	−32.90	−5.54	3.38	SAD
MPI-ESM1-2-LR	r1i1p1f1	18.88	−30.02	−5.67	3.46	SAD
CanESM5-CanOE	r1i1p2f1	12.04	−48.26	−5.81	6.37	SAD
CNRM-CM6-1-HR	r1i1p1f2	9.79	−60.55	−5.93	5.05	SAD
CanESM5	r1i1p1f1	12.28	−49.83	−6.12	6.25	SAD
FGOALS-f3-L	r1i1p1f1	21.04	−29.43	−6.19	4.09	SAD
GFDL-CM4	r1i1p1f1	13.00	−50.24	−6.53	4.28	SAD
CNRM-ESM2-1	r1i1p1f2	14.00	−47.49	−6.65	4.49	No group
MIROC-ES2L	r1i1p1f2	12.79	−53.26	−6.81	3.59	No group
HadGEM3-GC31-MM	r1i1p1f3	13.53	−52.09	−7.05	5.53	No group
CMCC-CM2-SR5	r1i1p1f1	18.42	−38.97	−7.18	4.70	No group
CNRM-CM6-1	r1i1p1f2	13.56	−52.98	−7.19	5.01	No group
UKESM1-0-LL	r1i1p1f2	15.93	−45.97	−7.32	6.06	No group
HadGEM3-GC31-LL	r1i1p1f3	16.75	−46.30	−7.75	5.70	No group
CMCC-ESM2	r1i1p1f1	18.56	−42.24	−7.84	4.63	No group
MIROC6	r1i1p1f1	15.51	−53.79	−8.35	3.36	No group
GFDL-ESM4	r1i1p1f1	16.56	−52.17	−8.64	3.30	No group
ACCESS-ESM1-5	r1i1p1f1	21.27	−41.06	−8.73	4.26	LAD
ACCESS-CM2	r1i1p1f1	20.11	−44.11	−8.87	4.97	LAD
GISS-E2-2-G	r1i1p3f1	20.89	−53.91	−11.26	3.69	LAD
NorESM2-MM	r1i1p1f1	19.82	−64.66	−12.82	3.43	LAD
MRI-ESM2-0	r1i1p1f1	19.27	−72.79	−14.03	3.94	LAD
NorESM2-LM	r1i1p1f1	20.13	−70.25	−14.14	3.33	LAD
CESM2-WACCM	r1i1p1f1	21.40	−68.29	−14.61	5.10	LAD
FGOALS-g3	r1i1p1f1	32.84	−45.15	−14.83	3.27	LAD
CESM2	r10i1p1f1	21.77	−69.80	−15.19	4.94	LAD
GISS-E2-1-G	r1i1p1f2	22.89	−74.20	−16.98	4.21	LAD

hereafter referred to as small AMOC decline ("SAD"), while the models belonging to the group in which the AMOC declines more are hereafter referred to as large AMOC decline ("LAD"). The remaining 10 models display intermediate values of the AMOC decline and do not belong to any group. In this study, we define the AMOC strength index as the maximum value of the overturning streamfunction at 45°N and below 500-m depth. To assess the sensitivity of our results to the choice of the reference latitude for the AMOC strength definition, we also computed the AMOC index at 26.5°N and in the range 20°–50°N. While minor differences were observed in the group compositions, our findings remained consistent. Figure 1 shows time series of the AMOC strength, and models are coded with line types based on which group they belong to. Detailed information on the AMOC strength changes in each model is also provided in Table 1. The corresponding AMOC strength changes calculated at 26.5°N are provided in Table S1 in the online supplemental material for reference. To test the intermodel agreement and assess whether differences in simulated climate change are statistically significant between LAD and SAD groups, we perform the Student's two-tailed t test in the spatial maps. Where the test indicates that the differences are statistically significant, we argue that the driver of the differences between the two groups is the different amount of the AMOC decline. Further, we normalize changes in precipitation and atmospheric circulation of each model by its corresponding global-mean near-surface air temperature change ΔGMTAS, so that changes are shown per degree of global warming. We note that dividing by ΔGMTAS also reduces the influence of the global climate feedback on our results, helping to isolate the effect of the AMOC on ITCZ changes by mitigating the response to increased CO_2. Thus, where statistically significant, we deem the differences in simulated precipitation impacts to arise from the difference in the AMOC decline (cf. Bellomo et al. 2021). Alternatively, we also conduct a bootstrap test to further check whether the differences between the two groups of models are significantly different from the 1000 differences of two randomly chosen groups, and results are consistent with the t test.

For what concerns the abrupt 4xCO_2 and the PI-fixed AMOC experiments with EC-Earth3, we compute changes as the difference between time means over model years 50–150, covering years in which the weakened AMOC strength is nearly steady, and the corresponding control climate, here defined as long-term means of the whole piControl run (500-yr period). Again, we perform the Student's t test (at the 90%

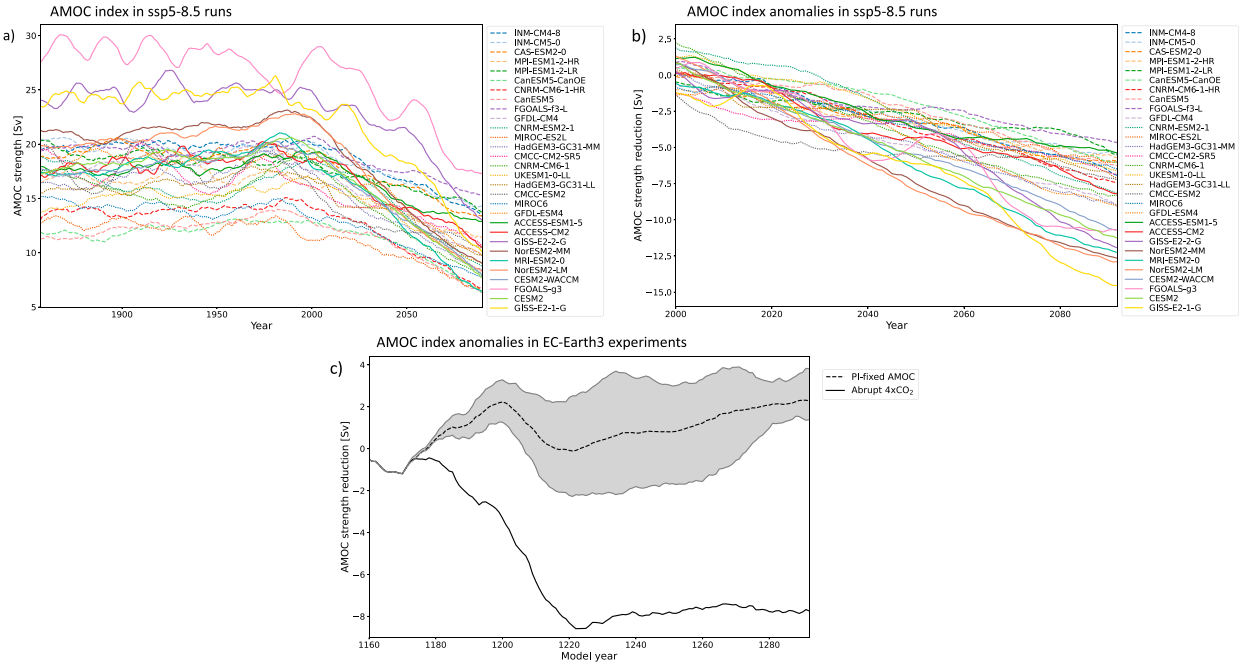

FIG. 1. The annual-mean AMOC strength index at 45°N: (a) time series between years 1850 and 2090 for the 30 CMIP6 models and (b) the corresponding AMOC index anomalies with respect to their climatology. Solid curves represent models in the LAD group. Dashed curves represent models in the SAD group. Dotted lines represent models not belonging to any group. In (c), black curves represent the AMOC index anomalies in EC-Earth3 abrupt 4xCO_2 (solid) and PI-fixed AMOC (dashed) experiments. The mean AMOC strength in the piControl run is 16.4 ± 2.6 Sv. The gray shading around the black dashed curve represents the PI-fixed AMOC ensemble spread. A 15-yr running mean has been applied to all time series. The AMOC index has been calculated as the maximum value of the overturning streamfunction at 45°N and below 500 m of depth.

significance level) between the control and the idealized experiments time series, to ensure that changes are not part of the model's internal climate variability. Time series of the AMOC strength in the EC-Earth3 experiments are also shown in Fig. 1. While in the SSP5–8.5 simulations, the AMOC decline was a consequence of CO_2 increase, in these idealized experiments, we attribute the precipitation impacts to the AMOC weakening by computing the difference between the 4xCO_2 and the PI-fixed AMOC experiment. To be consistent with the analysis of the SSP5–8.5 simulations, we also normalize changes in ad hoc EC-Earth3 experiments by ΔGMTAS. We perform the Student's t test between the abrupt 4xCO_2 and the PI-fixed AMOC model's years (100-yr period, from years 50 to 150) to ensure differences in simulated climate between the experiments do not derive from the EC-Earth3 model's internal climate variability.

To investigate the role of a weakening AMOC in shifting the ITCZ in the meridional direction, we evaluate the correlation coefficient and the strength of the linear regression between the magnitude of the AMOC decline and the difference in net precipitation ($P - E$) anomalies in two adjacent areas in the Atlantic deep tropics, where the $P - E$ change differences between the models are the strongest (see boxes in Fig. 3d). These regions are meridionally displaced and have coordinates 30°–8°W, 12°–3°N and 47°–25°W, 3°N–6°S. We compute the differences as the area-averaged $P - E$ anomalies in the southern box minus those in the northern box. Thus, positive values indicate a southward migration of the climatologically wetter region, while negative values indicate an intensification of the maximum of $P - E$. Our results are similar if we choose slightly different regions for the two boxes.

c. *Moisture budget*

To investigate the mechanisms driving changes in $P - E$, we perform the atmospheric moisture budget as derived in D'Agostino and Lionello (2020). Below, we provide a short overview of the method and refer the reader to that study and the references therein for a more in-depth derivation. Anomalies in the moisture budget are computed by monthly mean outputs, and the following equation is used:

$$\rho_w g \Delta(\overline{P} - \overline{E}) \approx \underbrace{-\int_0^{\overline{p}_s} (\overline{\mathbf{u}}_{\text{control}} \cdot \nabla \Delta\overline{q} + \Delta\overline{q} \nabla \cdot \overline{\mathbf{u}}_{\text{control}})\, dp}_{\Delta\text{TH}} + \underbrace{-\int_0^{\overline{p}_s} (\Delta\overline{\mathbf{u}} \cdot \nabla \overline{q_{\text{control}}} + \overline{q_{\text{control}}}\, \nabla \cdot \Delta\overline{\mathbf{u}})\, dp}_{\Delta\text{DY}} + (\Delta\text{TE} + \Delta\text{NL}) + \Delta S, \quad (1)$$

where P is the precipitation, E is the evaporation, $\mathbf{u}$ is the wind vector, q is the specific humidity, p_s is the surface pressure field, ρ_w is the density of water, and g is the gravity acceleration.

Overbars indicate monthly means, and primes indicate deviations from the monthly mean. Here, Δ denotes differences between the simulations (i.e., SSP5–8.5, PI-fixed AMOC, and abrupt 4xCO_2) and their reference control climatology (i.e., historical, piControl).

Through Eq. (1), we can decompose $P - E$ change as the sum of four drivers. The thermodynamic contribution ΔTH reflects changes in the mean humidity and includes changes of humidity gradient along the direction of the mean flow and changes of mean humidity in areas of mean flow convergence or divergence (i.e., constrained by the Clausius–Clapeyron relation). The dynamic contribution ΔDY involves changes in the mean meridional circulation and moisture transported by the mean wind flow. The transient eddies ΔTE and nonlinearities ΔNL are instead due to changes in the covariance of submonthly humidity and wind anomalies. Since the ΔTE + ΔNL term cannot be computed explicitly from monthly data, we have used the approach of D'Agostino and Lionello (2020), where it is estimated as

$$\Delta\mathrm{TE} + \Delta\mathrm{NL} = \rho_w g \Delta(\overline{P} - \overline{E}) - \Delta\left[\nabla \int_0^{\overline{p_s}} \overline{\mathbf{u}} \cdot \overline{q}\, dp\right], \tag{2}$$

while the surface contribution ΔS is computed as the residual:

$$\Delta S \approx -\Delta\left[\nabla \int_0^{\overline{p_s}} \overline{\mathbf{u}} \cdot \overline{q}\ dp\right] - \Delta\mathrm{TH} - \Delta\mathrm{DY}. \tag{3}$$

To estimate the AMOC influence on each of these contributions to the total $P - E$ change, we compute the anomalous moisture budget for both the SAD and LAD groups and the PI-fixed AMOC and the 4xCO_2 experiments; then, we analyze the respective differences. Concerning the SAD and LAD groups, we consider changes significant if at least two-thirds of the models agree in the sign of change. We note that for the GISS-E2-1-G, we encountered unrealistic fluxes over land; hence, for this model, we included only values over the ocean.

d. *Tropical Atlantic meridional atmospheric overturning circulation*

We investigate the dynamic contribution of the atmospheric mean flow over the tropical Atlantic Ocean with an analysis of the atmospheric mass streamfunction, which is closely related to the mean Hadley circulation. To compute the meridional streamfunction in a regional domain (i.e., in the Atlantic sector), the assumption of nondivergent meridional circulation, which is essential to ensure mass conservation in the computation of the Stokes streamfunction, is invalid. Thus, we follow the approach of Zhang and Wang (2013), Schwendike et al. (2014), and Nguyen et al. (2018) to partition the three-dimensional circulation into two divergent circulations lying in orthogonal planes that satisfy continuity independently. Through the Helmholtz decomposition, we extract the irrotational component of the meridional wind flow (i.e., the only contribution to the vertical flow), which can be regarded as the meridional overturning circulation. The Hadley overturning can be represented by a streamfunction computed from the divergent meridional wind similar to the Stokes streamfunction:

$$\psi_y(y, p) = \frac{2\pi R \cos y}{g} \int_{p_t}^{p_s} [v_d(y, p)]\, dp,$$

where R is Earth's radius, g is the standard gravity, p_t is pressure at the top of the troposphere, p_s is the surface pressure field, v_d is the divergent meridional wind, and y is the latitude. Brackets refer to a zonal average over a specified limited domain. In this study, we select longitudes ranging between 60°W and 10°E.

3. Results

a. *AMOC circulation change*

The time series of the annual-mean AMOC index at 45°N in all the SSP5–8.5 simulations reveal a substantial AMOC weakening occurring by the end of the current century, although a great intermodel spread exists (Fig. 1). The highest AMOC decline corresponds to a change in strength of about −74%, and the lowest change is about −11%. The mean change of all models corresponds to about −47% of AMOC strength reduction, with a median of −49%. In Fig. 1, solid curves represent the models in which the amount of AMOC reduction belongs to the lower tercile of the distribution of all models (LAD models, AMOC reduction ranges from −8.7 and −17.0 Sv). The dashed curves, on the other hand, represent the models that belong to the upper tercile (SAD models, AMOC reduction ranges from −0.9 and −6.5 Sv). Dotted colored lines represent models in the middle of the range of AMOC declines and do not belong to any groups. Note that models belonging to the LAD group (i.e. models in which the AMOC declines more) also exhibit a stronger AMOC in the climatology (c.f. solid contours in Fig. 2), which is consistent with previous studies (e.g., Weijier et al. 2020). As expected, the EC-Earth3 PI-fixed AMOC experiment (dashed black curve) is the only simulation where the AMOC strength, despite increasing greenhouse gases in the background, does not decrease. On the contrary, in the EC-Earth3 abrupt 4xCO_2 simulation (solid black curve), the AMOC decreases significantly (∼ −7.6 Sv of change, corresponding to a 46% reduction). A decline of 7.6 Sv is comparable with that of models belonging to no group (see Table 1).

Figure 2 shows the changes in the meridional oceanic mass streamfunction in a transect of the Atlantic ocean between 30°S and 70°N in the SAD group (Fig. 2a), in the LAD group (Fig. 2b), in the PI-fixed AMOC experiment (Fig. 2c), and in the abrupt 4xCO_2 experiment (Fig. 2d). The reduction of the AMOC circulation strength in the LAD group is much larger than in the SAD group everywhere and statistically significant at the 90% level. The transect shown in Fig. 2c shows that the AMOC circulation does not undergo any notable reduction in the PI-fixed AMOC experiment, differently from the abrupt 4xCO_2 experiment, where the magnitude of the AMOC reduction is strong and extends to the entire Atlantic basin.

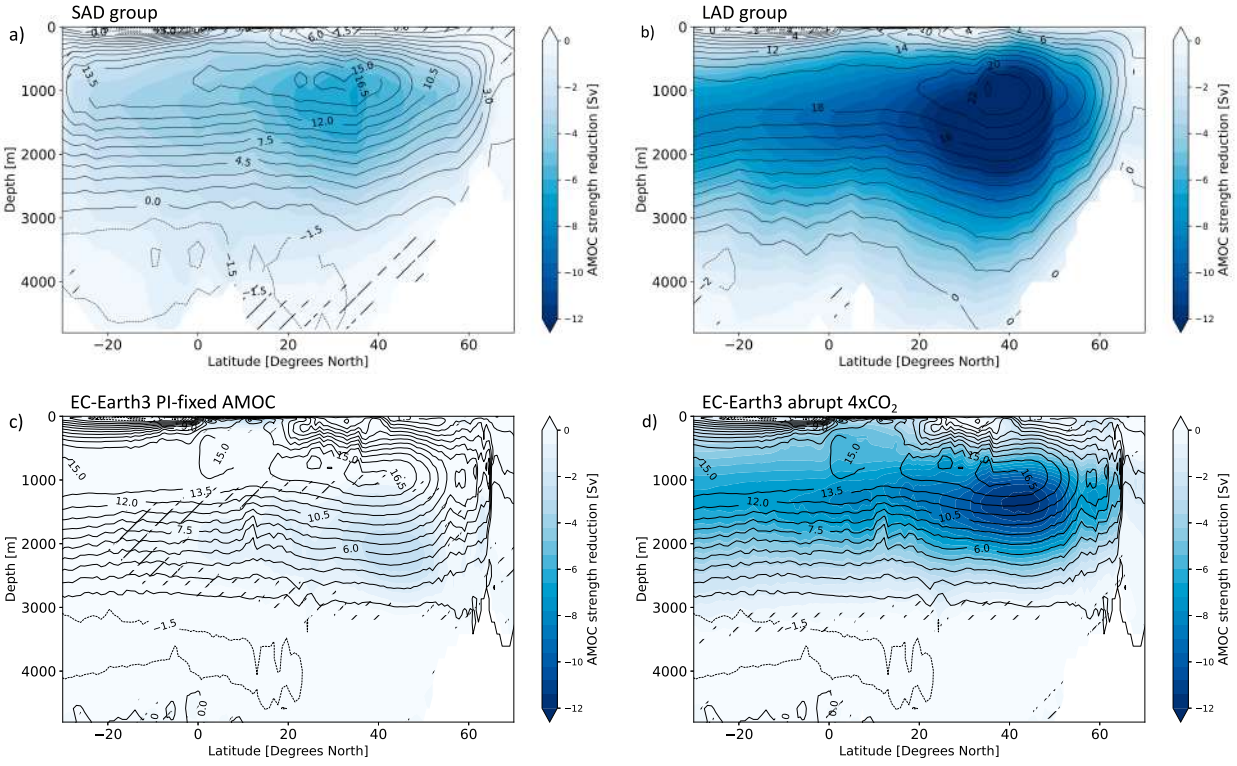

FIG. 2. Oceanic mass streamfunction change in the Atlantic sector. For the (a) SAD and (b) LAD groups, changes are evaluated between the SSP5–8.5 simulations and the historical simulation. Black contours represent the respective climatologies. For (c) the PI-fixed AMOC and (d) the abrupt 4xCO_2 experiments, changes are evaluated with respect to the piControl run (black contours). In all panels, hatches indicate areas where the statistical *t* test on the ocean mass streamfunction change with respect to the reference climatology is not statistically significant at the 90% confidence level.

b. Net precipitation change in SAD and LAD groups

In the SAD group (Fig. 3a), $P - E$ intensifies over the ocean close to the western African coast but decreases all over the Atlantic sector and the Amazon. Overall, models with a small AMOC decline project a drying tendency of the climatological ITCZ (here, intended as the tropical region where the annual-mean moisture convergence occurs, ie., the moisture ITCZ), over the western side of the Atlantic basin and an intensification over the eastern side at positive latitudes resulting in a drier tropical Atlantic equator. We note that this thermodynamic constraint is less robust over land, as reported in previous studies (Byrne and O'Gorman 2015). In contrast, the LAD group (Fig. 3b) exhibits a southward shift in $P - E$, featuring increased $P - E$ right at the equator and drying tendencies at higher latitudes. The maximum of the tropical Atlantic precipitation change (Fig. 3b) is displaced westward with respect to the climatological maximum, consistent with previous studies suggesting it could be related to the eastern Pacific Ocean anomalous warming under future climate change (Nicknish et al. 2023). Hence, when the multimodel mean is taken (Fig. 3c), the change in net precipitation shows a mix of these two patterns. The $P - E$ shows a slight increase below the climatological maximum, specifically between the equator and 4°N, while it decreases in the subtropics. Figure 3d displays the LAD minus SAD $P - E$ change, which better highlights the role of a relatively larger AMOC decline. LAD models show a substantially drier tropical ocean between 4° and 10°N. At the same time, a large band of positive values from 4°N toward southern latitudes indicates a diffused wetter climate for the LAD group relative to the SAD group. Major differences occur in the deep tropics, further confirming a southward ITCZ migration in the LAD group, which is absent in the SAD group.

Although the model grouping is based on the reduction of mass transport (i.e., strength of the overturning mass streamfunction change at 45°), further analyses (not shown) suggest that both model groups experience a reduction in oceanic heat transport, though this is more pronounced for the LAD group. The lack of an ITCZ shift in SAD models may be explained by other mechanisms constraining its meridional position (Bischoff and Schneider 2014; Schneider et al. 2014), making the signal unclear when the oceanic heat transport is reduced but only to a limited extent. In contrast, a more significant reduction shows a net southward shift that is consistent across LAD models.

To better investigate the intermodel spread in the ITCZ response, in Fig. 4a, we show the difference in normalized $P - E$ change between the north and south boxes (see

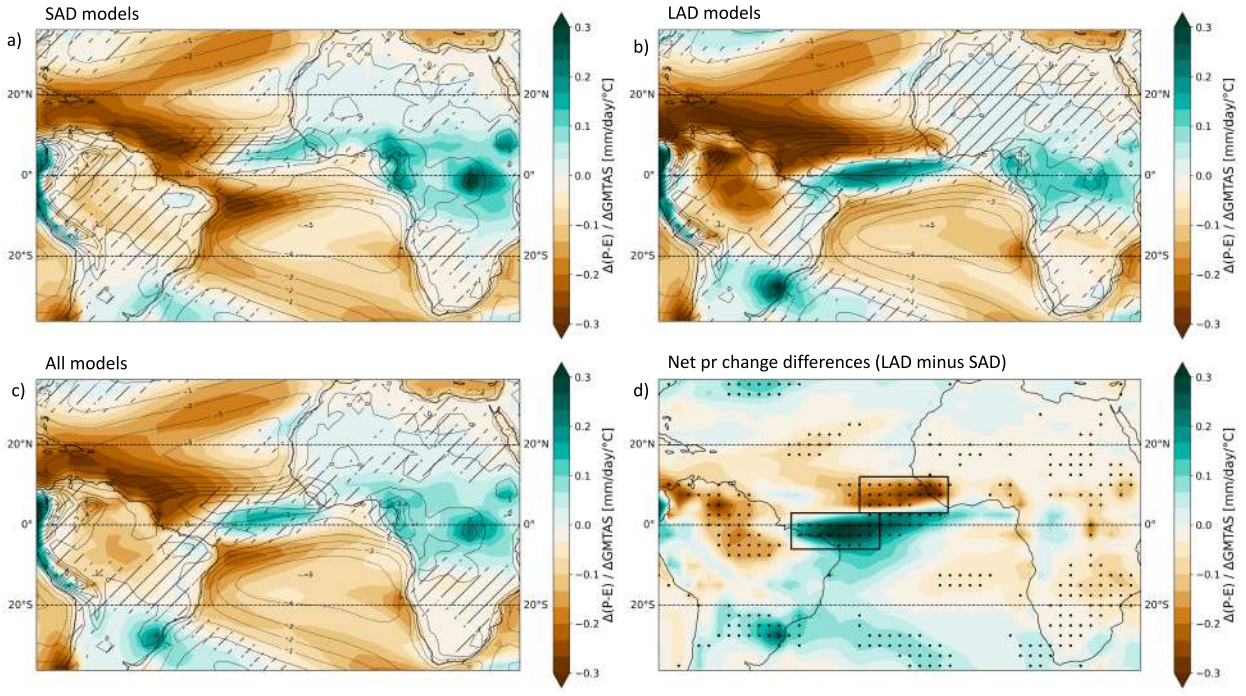

FIG. 3. Normalized annual-mean net precipitation change in SSP5–8.5 scenario projections for (a) the SAD group, (b) the LAD group and (c) all models. Superimposed contours show the mean annual $P - E$ climatology computed as the ensemble mean of the historical run from all models. Hatches indicate areas where the difference between historical and future $P - E$ is not statistically significant at the 90% confidence level, based on the Student's t test. (d) Difference between the LAD and the SAD $P - E$ change. Stippling indicates areas where the difference in $P - E$ change between the LAD and SAD ensemble means is statistically significant at the 95% confidence level of the Student's t test.

Fig. 3d) against the AMOC change for each model. Positive values in Fig. 4a indicate a southward shift of the moisture ITCZ over the Atlantic, while negative values indicate an intensification of the climatology. Most LAD models exhibit positive values, while most SAD models display negative values, indicating a clear division. We use the same boxes to evaluate differences in $P - E$ change in the EC-Earth3 abrupt 4xCO_2 experiment (red star in Fig. 4a) and note that the ITCZ changes fall within the models not belonging to the SAD or LAD groups.

We perform both a robust Hubert regression ($y = -0.04 \times -0.332$) with a R^2 of 0.72 (Fig. 4a, blue line), which excludes outliers, and a linear regression analysis ($y = -0.045 \times -0.351$, not shown), with a statistically significant R^2 of 0.72, which includes all models except for the abrupt 4xCO_2 EC-Earth3 experiment. The regression analysis supports the importance of intermodel differences in the AMOC decline in shaping tropical precipitation spatial distribution. Specifically, larger AMOC declines result in a more pronounced southward shift of the moisture ITCZ over the Atlantic, being therefore a fundamental factor to understand projected future changes. Moreover, Fig. S1 shows $P - E$ change regressed onto the AMOC decline, further supporting this result. We also note that results are similar if we use precipitation instead of $P - E$ (Fig. S2).

Figure 4b shows the zonal-mean $P - E$ changes for the SAD (thick red curve) and the LAD (thick blue curve) groups, compared to the climatological zonal-mean $P - E$ (black curve), averaged over the year and the Atlantic sector. As expected, the climatology displays a peak around 5°N, corresponding to the annual-mean location of the ITCZ. In the SAD ensemble, positive anomalies near the ITCZ suggest a slight strengthening of the climatological peak of $P - E$ in that region. Conversely, a large AMOC decline leads to negative anomalies at 5°N but positive anomalies at the equator, corroborating a southward shift of the Atlantic ITCZ. The zonal-mean $P - E$ change differences (green line, markers indicate statistical significance at each latitude) better show the substantial role of a stronger AMOC decline in displacing southward the positive $P - E$ changes in the tropical Atlantic.

c. *Mechanisms of net precipitation change in SAD and LAD groups*

Changes in $P - E$ appear to be driven by different processes depending on how much the AMOC declines. To investigate these mechanisms, we apply an atmospheric moisture budget to model data (cf. D'Agostino and Lionello 2020). This allows us to separate thermodynamic ΔTH from dynamic contributions ΔDY and to further quantify changes resulting from transient eddies and nonlinearities ΔTE + ΔNL.

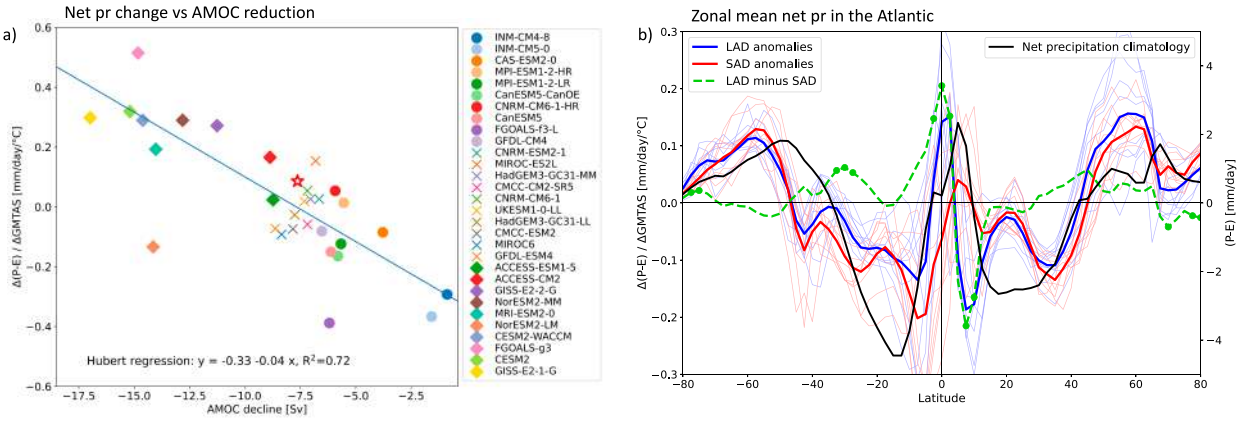

FIG. 4. Meridional displacement of zonal-mean tropical Atlantic net precipitation in its annual-mean in SSP5–8.5 scenario projection. (a) Normalized $P - E$ change difference between the two boxes in Fig. 3d (south box minus north box), against the AMOC reduction expressed in Sverdrups. Circles indicate the SAD models, diamonds indicate the LAD models, crosses indicate the other models, while the red star represents the EC-Earth3 abrupt $4xCO_2$ experiment. The blue line is the Huber regression (i.e., robust to outliers) on all models excluding the $4xCO_2$ EC-Earth3 simulation. (b) Zonal-mean annual $P - E$ in the Atlantic sector (between 35° and 5°W): the black curve shows the climatological $P - E$ computed from all the historical simulations; the red curves show $P - E$ change for the members of the SAD group and the SAD group ensemble mean (thicker red curve); the blue curves show $P - E$ change for the members of the LAD group and the LAD group ensemble mean (thicker blue curve); and the green curve shows the difference between the two groups. Markers on the green curve indicate where the differences between the SAD and LAD groups are statistically significant with the 95% confidence level of the Student's t test.

Since ΔTE + ΔNL and the residual are small, in the main text, we only show ΔTH and ΔDY, while the other terms can be found in Fig. S3. Focusing on changes over the ocean, Figs. 5a–c display consistent spatial patterns of $P - E$ change, indicating that the ΔTH term contributes primarily by intensifying the hydrological cycle (e.g., Held and Soden 2006). The strength of anomalies is slightly different among these panels, although the normalization by ΔGMTAS helps to limit this effect. It is worth noting that LAD models exhibit more warming in the tropical Atlantic compared to SAD models, implicating stronger thermodynamic changes (cf. Figs. 5b,c). Nevertheless, we can conclude that ΔTH drives precipitation impacts independently of the amount of AMOC weakening in these models.

In contrast, the ΔDY term shows substantial differences among the three panels (Figs. 5d–f). In "all models" (Fig. 5d),

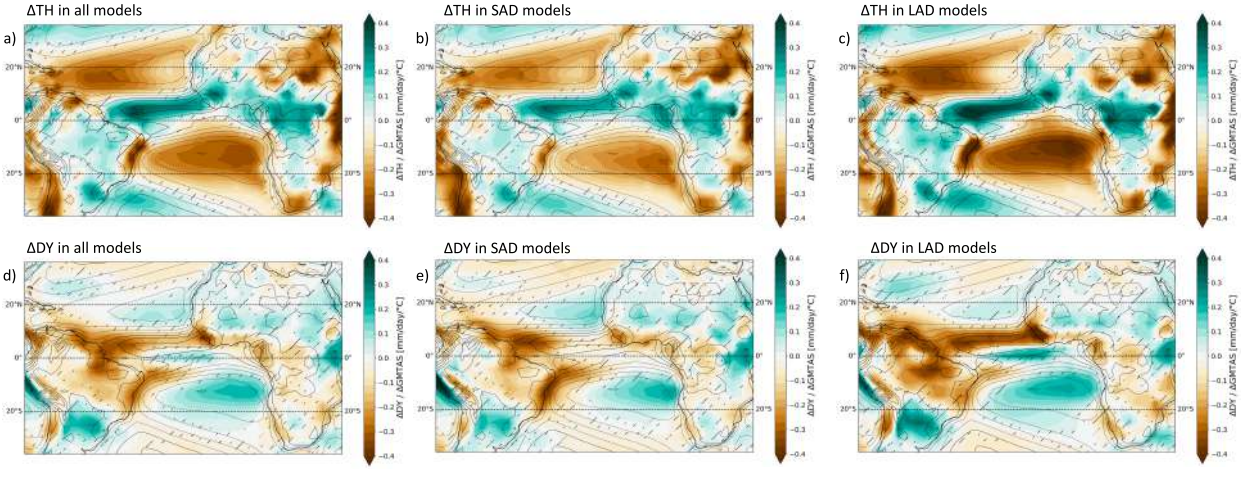

FIG. 5. Normalized annual-mean thermodynamic and dynamic drivers of net precipitation change in SSP5–8.5 scenario. ΔTH for (a) all models, (b) the SAD group, and (c) the LAD group. (d),(e),(f) As in (a),(b),(c), but for the ΔDY term. Note that the sum of these two contributions plus the contribution given by transient eddies and surface quantities (provided in SI Fig. S3) equals the $P - E$ change displayed in Fig. 3 by construction. Hatches indicate regions of intermodel disagreement, that is, where less than two-thirds of the models agree on the sign of the change. Superimposed contours show the mean annual $P - E$ climatology computed as the ensemble mean of the historical run from all models.

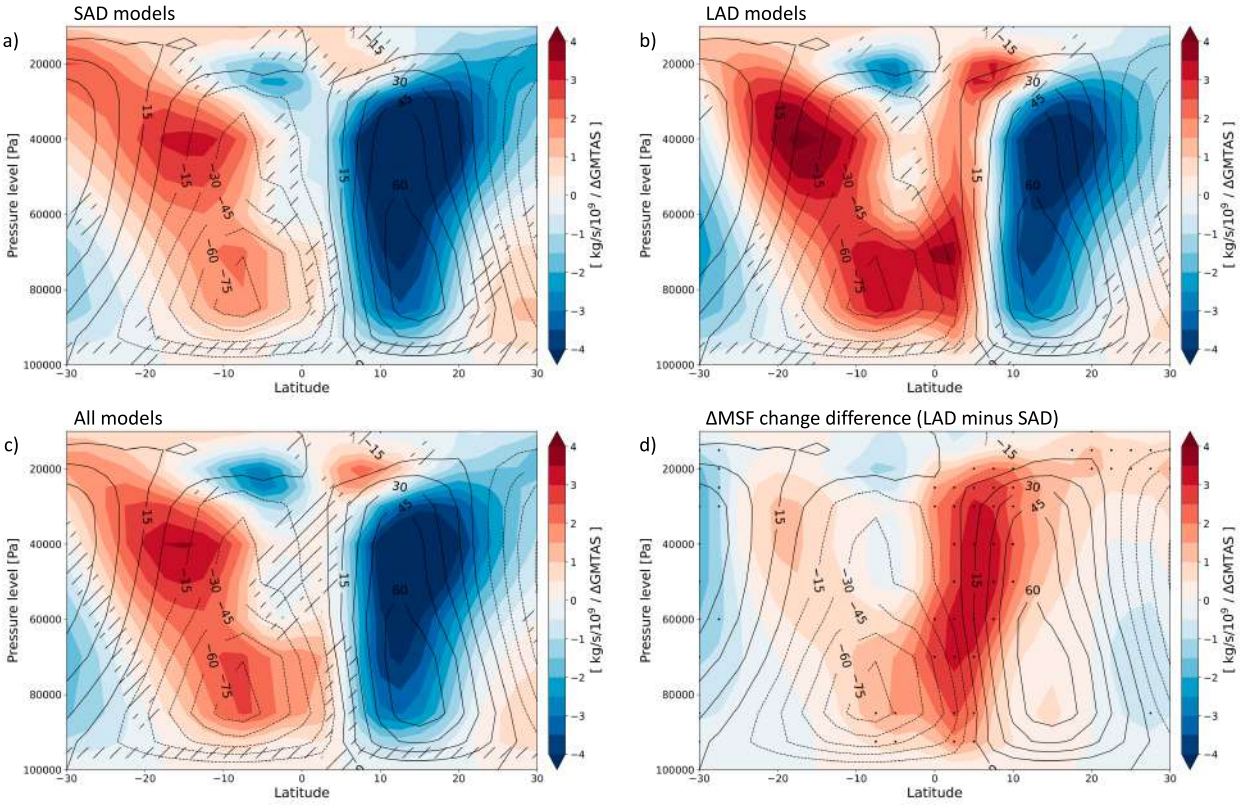

FIG. 6. Normalized annual-mean Atlantic atmospheric mass streamfunction changes in SSP5–8.5 scenario projections for (a) the SAD group, (b) the LAD group and (c) all models. The streamfunction is calculated on longitudes ranging from 60°W to 10°E. Superimposed contours show climatology computed as the ensemble mean of the historical run from all models. Hatches indicate areas where the difference between historical and future Atlantic atmospheric mass streamfunction is not statistically significant at the 90% confidence level, based on the Student's *t* test. (d) Difference between the LAD and the SAD atmospheric circulation anomalies. Stippling indicates areas where atmospheric circulation change differences between the LAD and SAD ensemble means are statistically significant with the 90% confidence level of the Student's *t* test.

a zonal asymmetry appears between 35° and 10°W, along with a drying tendency near the coasts of South America. This pattern represents the average effect of various processes. Specifically, the SAD group (Fig. 5e) displays a strong dynamical drying signal near the eastern South American coasts, extending throughout the deep tropics of the Atlantic and intensifying toward the Gulf of Guinea. Instead, the dynamic component of the LAD group (Fig. 5f) exhibits a meridional dipole-like structure located between the equator and 10°N, resembling the all models panel but with stronger anomalies at the equator. Furthermore, we observe similarities between Figs. 3a and 5e ($P - E$ changes and ΔDY for the SAD group), particularly the drying signal along the American coasts, and between Figs. 3b and 5f, showing the (dynamical) equatorial moistening displayed by the LAD ensemble. These findings underscore the substantial impact of dynamic drivers on the $P - E$ changes in the tropical Atlantic. In the case of a smaller AMOC decline, the deep tropical Atlantic experiences dynamic drying, while a larger AMOC decline favors ΔDY-induced moistening of the equator, achieved through the southward migration of the ITCZ (cf. Fig. 4a).

d. *Atlantic atmospheric overturning circulation change in SAD and LAD groups*

The dynamic term ΔDY appears to play a prominent role in causing differences in $P - E$ changes between the SAD and LAD groups. Because ΔDY quantifies changes in the column-integrated moisture transported by the mean flow, which in the tropics mostly occurs in the lower branches of the Hadley cells, here, we investigate changes in the meridional overturning atmospheric mass streamfunction across longitudes ranging from 60°W to 10°E. To achieve this, we adopt the approach outlined by Zhang and Wang (2013) and further developed by Schwendike et al. (2014) and Nguyen et al. (2018), which allows us to evaluate the streamfunction over a limited longitudinal range ensuring mass conservation (see methods). Figures 6a and 6b show the Atlantic mass streamfunction changes ΔMSF for the SAD and LAD groups, respectively. Superimposed black contour lines represent the mean atmospheric circulation computed from the historical simulation of all models. The climatological ascending branches of the Northern and Southern Hemisphere annual-mean Hadley cells converge at around 5°N, roughly corresponding to the meridional position

of mean annual peak of Atlantic precipitation. We now focus on this region and nearby latitudes to explore changes in the mass streamfunction associated with changes in the position of the ITCZ.

In the LAD group (Fig. 6b), positive (clockwise) anomalies between the equator and 5°N indicate that the Northern Hemisphere cell strengthens close to the equator, whereas the Southern Hemisphere cell weakens. Specifically, the clockwise anomalies at the interface between the two cells suggest a squeezing of the climatologically cross-equatorial mean annual Southern Hemisphere cell southward, while the Northern Hemisphere cell expands. We note that the SAD group (Fig. 6a) does not show significant changes in cell intensity in this region. Instead, both the SAD and LAD groups exhibit a broad weakening of the Hadley cells, reflecting the slowdown of the tropical overturning circulation in a warming climate (cf. Lu et al. 2007; Byrne et al. 2018).

Figure 6d (LAD minus SAD) shows statistically significant differences in the change of the strength of the Atlantic Hadley cells across the entire atmospheric column from the equator to ~9°N, extending northward at higher altitudes (i.e., above 30 hPa). Discrepancies at higher altitudes indicate a difference in the rise of the tropopause height. In general, models with stronger AMOC weakening also show more intense tropical warming (Bellomo et al. 2021), resulting in enhanced deepening of tropical convection and heightening of the Hadley cell (Neelin and Held 1987), hence such significant differences. While differences in the tropopause height changes can be attributed to differences in the tropical warming, we argue that differences in the strength and structure at tropical latitudes and lower elevation of the Atlantic Hadley cells are driven by the intermodel spread in the AMOC response to climate change.

In LAD models, the reduction in cross-equatorial ocean heat transport caused by the weakened AMOC influences the Atlantic Hadley circulation, possibly leading to a southward shift of the ascending branch in its annual mean (i.e., the Southern Hemisphere Hadley cell tends to become less cross equatorial). Thus, the dynamical ΔDY contribution to the meridional displacement of $P - E$ change (i.e., the southward shift of the Atlantic ITCZ) may be explained by changes in the Atlantic atmospheric overturning circulation in the group of models featuring a relatively larger AMOC decline. We note that when evaluated globally, the atmospheric circulation anomalies show a similar pattern of change, but differences between the groups at 5 °N are not statistically significant (Fig. S4), suggesting less influence of the AMOC on the ITCZ on a global scale. Similar changes in the Hadley cells are consistent with previous studies analyzing idealized experiments where the AMOC is artificially shut down (Orihuela-Pinto et al. 2022; Bellomo et al. 2023), lending confidence that our results are robust.

e. *Net precipitation changes in the EC-Earth3 idealized experiments*

Figures 7a and 7b depict $P - E$ changes in the Atlantic sector in the PI-fixed AMOC and the abrupt 4xCO_2 experiment, respectively. The changes are normalized by ΔGMTAS, as in Fig. 3, to facilitate a comparison between them. The $P - E$ changes show a very similar spatial pattern between the two experiments. The moisture ITCZ tends to dry out, while positive anomalies are shifted both northeast and southwest with respect to the climatological peak of $P - E$ under increasing greenhouse gases in the EC-Earth3 model. The zonal-mean Atlantic $P - E$ is shifted southward in the abrupt 4xCO_2 run (blue curve in Fig. 7c) compared to the PI-fixed AMOC experiment (red curve). This is highlighted by the green curve showing the difference between the two. Positive differences between 5°S and 5°N (with a peak between 2.5° and 5°N) indicate that in the abrupt 4xCO_2 the climate is wetter across the equator and southward with respect to the PI-fixed AMOC run. The green curve clearly resembles the one represented in Fig. 4b, although anomalies are located at different latitudes. The result corroborates the southward shift tendency of the anomalous Atlantic ITCZ mainly driven by a substantially weakened AMOC. Since, here, we analyze one model (EC-Earth3) and in Fig. 4b an ensemble of models, some differences are expected. But overall, both figures suggest a fingerprint of the AMOC decline on the southward shift of the ITCZ in a warming twenty-first century. Notably, a major effect of a strong AMOC slowdown as occurs in the abrupt 4xCO_2 simulation is the reduced warming in the subpolar North Atlantic (Liu et al. 2020; Bellomo et al. 2021) because the northward transport of heat by the ocean is reduced. Thus, in this experiment, the southward shift of the ITCZ reflects the altered interhemispheric energy transport.

Figure 7d (Fig. 7b minus Fig. 7a) quantifies the impacts of an AMOC weakening, showing a generally wetter moisture ITCZ and a wetting signal that expands toward the southwest direction (near the South American coast), following the southwest shift already observed for the LAD group anomalies (Figs. 3b,d). We note that the northeastern wetting seen in Figs. 7a and 7b is much stronger in the PI-fixed AMOC experiment, and no trace of it remains when assessing the difference between the two, meaning that in the abrupt 4xCO_2 run it is limited by the declining AMOC. The tongue of positive differences near the North African coast in Fig. 7d is caused by a strong cooling spot that occurs under the abrupt 4xCO_2 simulation. The cooling leads to reduced $P - E$ changes because the evaporation diminishes in response to lower temperature (see Bellomo and Mehling 2024). In fact, it does not appear when considering only precipitation anomalies (see Fig. S5d).

f. *Moisture budget in the EC-Earth3 idealized experiments*

As shown before, the ΔTH contribution to the moisture budget is an intensification of the present-day hydrological cycle. It is, therefore, not surprising that Figs. 8a and 8b showing the ΔTH contribution in the PI-fixed AMOC and the abrupt 4xCO_2 experiments exhibit a band of positive anomalies slightly north of the equator where the moisture ITCZ over the Atlantic lies in the EC-Earth3 piControl mean climate (black contours in Fig. 8), and negative anomalies are displaced

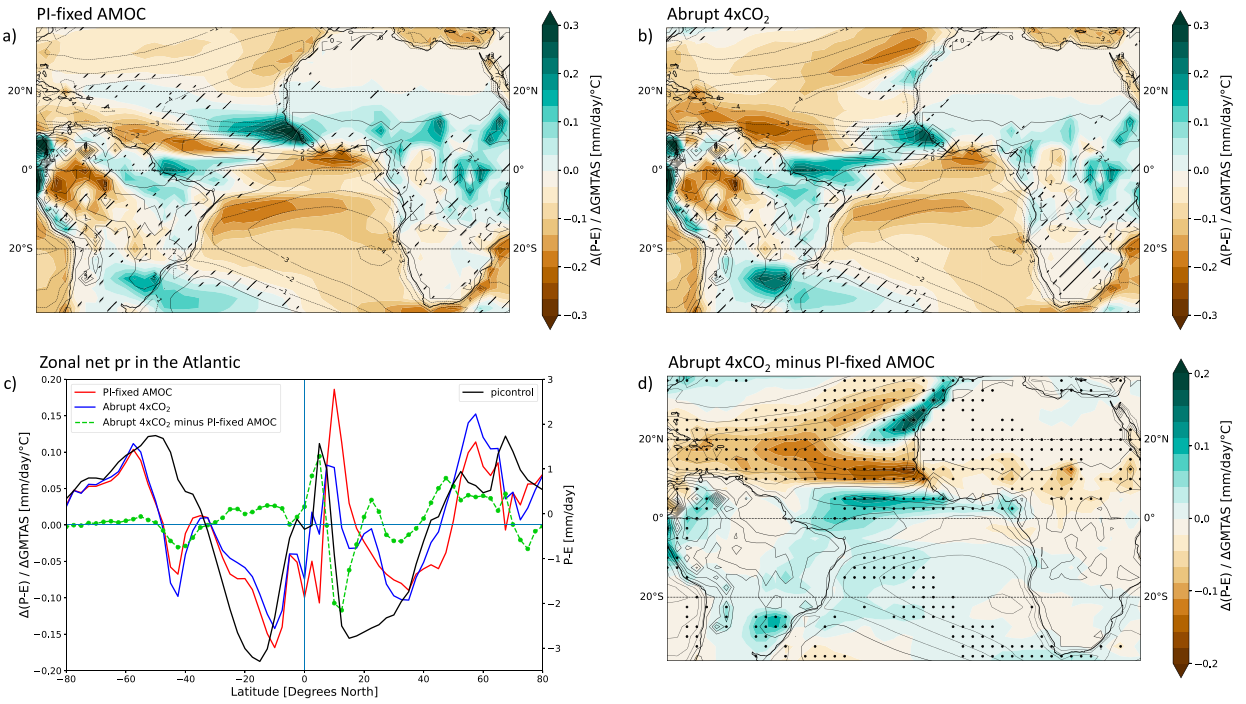

FIG. 7. Normalized annual-mean net precipitation changes in the EC-Earth3 idealized experiments: (a) PI-fixed AMOC and (b) abrupt 4xCO_2. Superimposed contours show the mean annual $P - E$ climatology. Hatches indicate areas where $P - E$ changes are not statistically significant at the 90% confidence level, based on the Student's t test. (c) Zonal-mean annual $P - E$ in the Atlantic sector (between 35° and 5°W): the red curve shows the change in the PI-fixed AMOC experiment, the blue curve shows the change from the abrupt 4xCO_2 experiment, the black curve represents the piControl climatology, and the green curve is the difference between the two experiments. Markers indicate where the differences are statistically significant with the 95% confidence level of the Student's t test. (d) Difference between the PI-fixed AMOC and the abrupt 4xCO_2 $P - E$ change. Stippling indicates where $P - E$ change differences of the two experiments are statistically significant at the 95% confidence level of the Student's t test.

further north and south of this band. Hence, the ΔTH term (Fig. 8c) fails to explain the differences in tropical Atlantic $P - E$ change seen in Fig. 7d. Although both the experiments feature the "wet-gets-wetter, dry-gets-drier" paradigm (Held and Soden 2006), the PI-fixed AMOC experiment reveals a stronger intensification of the hydrological cycle in the Northern Hemisphere. Strong differences are indeed found near the coasts of northern South America (leading to a tongue of positive differences already mentioned for Fig. 7c), North Africa, and in the African monsoon region. This is consistent with the aforementioned AMOC-driven cooling of the Northern Hemisphere in the abrupt 4xCO_2 simulation, which does not occur in the PI-fixed AMOC experiment.

The spatial distribution of the ΔDY contribution to the moisture budget (Figs. 8d,e) is similar in the two experiments. Both panels show a drying signal between 10°S and 10°N that is reminiscent of that seen in the ΔDY contribution derived from the all-models ensemble mean future projections (Fig. 5b), except for the positive anomaly being displaced near the South American coast in the EC-Earth3 experiments. Note that in the 4xCO_2, this positive signal is broader and more intense between the equator and South America. Figure 8f shows the ΔDY difference between the abrupt 4xCO_2 and PI-fixed AMOC experiments, which allows us to assess the weakened AMOC impact on the column-integrated atmospheric moisture transport. Between the two Hemispheres, a bipolar seesaw, with adjacent positive/negative differences that change in sign around 7°N, indicates a stronger dynamical moistening of the equatorial latitudes occurring in the abrupt 4xCO_2 experiment. Therefore, Fig. 8f demonstrates that an AMOC weakening alone causes changes in the atmospheric circulation that lead to a southward shift of the tropical moisture ITCZ, also in a 4xCO_2 forced warmer climate.

4. Discussion and conclusions

Previous studies have found that in climate change projections from the CMIP5 and CMIP6 models, there is large uncertainty in tropical Atlantic precipitation change, including the meridional dislocation of the ITCZ (e.g., Byrne et al. 2018; Mamalakis et al. 2021). One study (Good et al. 2022) based on results from one state-of-the-art climate model (HadGEM3) suggested that intermodel uncertainties in future tropical Atlantic precipitation change may stem from model biases, including the AMOC representation. Other studies have also indicated a potentially significant role for the AMOC in tropical Atlantic precipitation change (e.g., Zhang and Delworth 2005; Jackson et al. 2015; Bellomo et al. 2021; Liu et al. 2020;

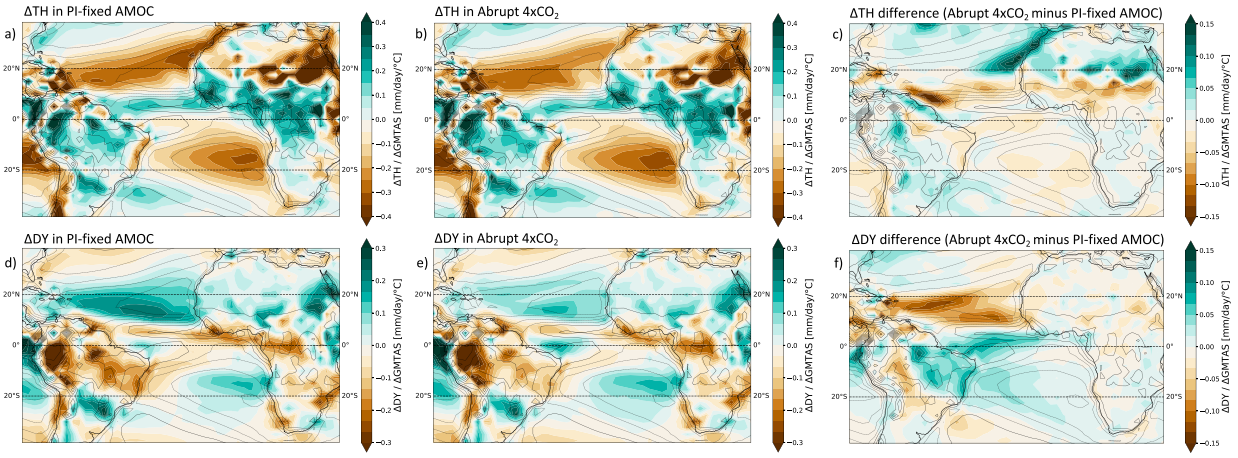

FIG. 8. Normalized annual-mean thermodynamic and dynamic drivers of net precipitation change in EC-Earth3 idealized experiments. (a),(b) ΔTH for the PI-fixed AMOC and the abrupt $4xCO_2$, respectively. (c) Their difference. (d),(e) ΔDY for the PI-fixed AMOC and the abrupt $4xCO_2$, respectively. (f) Analogous to (c), but for the ΔDY term. Note that the sum of these two contributions plus the contribution given by transient eddies and surface quantities (provided in SI Fig. S6) equals the $P - E$ change displayed in Fig. 7 by construction. Superimposed contours show the mean annual $P - E$ control climatology.

Nicknish et al. 2023), but our study specifically provides evidence supporting an important role for a weakened AMOC in driving tropical Atlantic $P - E$ changes in a warming twenty-first century climate. In this study, we used a high emission scenario (the SSP5–8.5 projections), as the large intermodel spread allowed us to statistically separate the response of the Atlantic ITCZ to different magnitudes of AMOC weakening. However, we would expect similar results even if a less extreme greenhouse gas increase scenario were used because Weijer et al. (2020) show that significant intermodel spread exists in the AMOC representation under other emission pathways as well. Because in these simulations the AMOC decline is forced by increasing greenhouse gases, although we took measures to only consider the AMOC impact and not the CO_2 forcing, we are not fully able to cleanly separate the effect of greenhouse gases from the effect of the AMOC decline on tropical Atlantic $P - E$ change. To overcome this difficulty, we additionally analyzed ad hoc experiments with the EC-Earth3 model. In these experiments, we artificially fixed the AMOC strength at preindustrial levels. With this additional analysis, we were able to attribute precipitation impacts to the AMOC decline alone. Our results suggest that the AMOC decline may be a key driver of intermodel spread in meridional displacement of tropical Atlantic ITCZ, and the models featuring a larger AMOC decline in the SSP5–8.5 experiment project a southward ITCZ displacement, while models featuring a smaller AMOC decline exhibit no shift. The EC-Earth3 experiments corroborate findings from the multimodel analysis. We performed an additional analysis at 26.5°N, a latitude where the AMOC exhibits a strong wind-driven component (Buckley and Marshall 2016), and obtained consistent results, though less significant. This analysis was motivated by the hypothesis that a weakening of the HC alone would reduce the northward Ekman contribution to the AMOC, thereby slowing it and driving a direct coupling with changes in the ITCZ. However, the agreement with findings at 45°N confirms that, while wind forcing plays a role, the observed ITCZ shifts are directly tied to the basin-scale AMOC slowdown. The ITCZ over the Pacific basin shows signals of a southward ITCZ shift as well. Nevertheless, the response in the Atlantic is clearer, while the effect in the Pacific is influenced by other effects related to climate change, making it harder to associate the differences in the meridional position to the spread of the AMOC decline. Finally, it remains open to explore other competing mechanisms that affect ITCZ displacement under simulation of future climate change, which may also amplify the intermodel spread. Indeed, while AMOC reduction is one factor at play, not all models show a southward shift of the ITCZ, despite all of them exhibiting a decrease in interhemispheric ocean heat transport.

To put our results in context, we recall that Byrne et al. (2018) examined an ensemble of 32 model simulations of the twenty-first century from the CMIP5 archive and found that the median model projected a northward shift of the global-mean ITCZ of 0.03° latitude per Kelvin of global-mean surface-air warming, with an interquartile range across models of $0.46° K^{-1}$. Of the models which they analyzed, 17 out of 32 predicted a northward ITCZ shift by the end of the twenty-first century, while the remaining models predicted a southward shift. This near-even split between models results in great uncertainty regarding the direction of the ITCZ shift by the end of the twenty-first century, which has significant implications for regional hydroclimate changes. In our study, we demonstrate that a southward shift of the Atlantic ITCZ is driven by changes in the mean meridional atmospheric circulation, specifically the Atlantic regional Hadley circulation, but only in models featuring a relatively larger AMOC decline. Although we did not specifically examine global-scale ITCZ changes, Fig. S4 indicates a southward shift of the Northern Hemisphere Hadley cell on a global scale in models with relatively larger AMOC declines.

Therefore, when comparing our results with Byrne et al. (2018) and the latest AR6 IPCC report (IPCC 2022), we posit that the intermodel spread in the meridional displacement of the ITCZ may, in part, be attributed to the intermodel spread in AMOC decline. Moreover, beyond meridional shifts, we observe that the AMOC decline also modulates the intensity, spatial structure, and zonal migrations of $P - E$ change. Recent studies (e.g., Nicknish et al. 2023) suggest that AMOC reduction, coupled with eastern equatorial Pacific warming, acts as a key driver of zonal and meridional energy flux shifts, which in turn mirror gross distributional changes of tropical precipitation. Therefore, differences in zonal shifts of $P - E$ between the two groups may arise from intermodel differences in eastern equatorial Pacific warming (cf. Bellomo et al. 2021), affecting trade wind patterns over the Atlantic. Our findings suggest that, under future global warming, the degree of compensation between thermodynamic (TH) and dynamic (DY) contributions, which is fundamental to understand future African monsoon precipitation (D'Agostino et al. 2019), is potentially impacted by the AMOC slowdown effect on DY. The SSP5–8.5 simulations also reveal that a significant weakening of the AMOC leads to reduced annual-mean rainfall in the Amazon region, which aligns with findings from idealized climate model experiments in which the AMOC is artificially suppressed (e.g., Vellinga and Wood 2002; Parsons et al. 2014; Jackson et al. 2015). However, the difference in precipitation change simulated by the EC-Earth3 experiments does not agree with this result; therefore, caution is needed when attributing it to the declining AMOC.

Finally, we assert that the AMOC plays a crucial role as a key driver of intermodel uncertainty in projections of future tropical Atlantic precipitation changes. Our study shows that targeted experiments are needed to specifically investigate climatic impacts of the AMOC decline relative to anthropogenic global warming. We also suggest that to understand the impacts of the AMOC on tropical Atlantic hydroclimate, continued observational campaigns (McCarthy et al. 2015; Frajka-Williams et al. 2019; Li et al. 2021) are essential. An observational constraint on the AMOC response to future climate change would be beneficial for reducing intermodel uncertainty in its impacts.

Acknowledgments. We acknowledge the World Climate Research Programme's Working Group on Coupled Modelling, which is responsible for CMIP, and we thank the climate modeling groups (listed in Table 1 of this paper) for producing and making available their model output. G. C., K. B., and J. v. H acknowledge funding from the European Union Next-Generation EU within the RETURN Extended Partnership (National Recovery and Resilience Plan – NRRP, Mission 4, Component 2, Investment 1.3 – D.D. 1243 2/8/2022, PE0000005). K. B. acknowledges funding from JPI Oceans and JPI Climate "Next Generation Climate Science in Europe for Oceans"–ROADMAP Project (D. M. 593/2016) and from the European Union's Horizon 2020 research and innovation program under the Marie Skłodowska-Curie Grant Agreement 101026907 (CliMOC).

Data availability statement. CMIP6 data are openly available in the CMIP6 Earth Science Grid Federation archive at https://esgf-data.dkrz.de/search/cmip6-dkrz/. Relevant dataset generated and analyzed for the Ec-Earth3 experiments during the current study is available at https://doi.org/10.5281/zenodo.11545299.

REFERENCES

Bellomo, K., and O. Mehling, 2024: Impacts and state-dependence of AMOC weakening in a warming climate. *Geophys. Res. Lett.*, **51**, e2023GL107624, https://doi.org/10.1029/2023GL107624.

——, M. Angeloni, S. Corti, and J. von Hardenberg, 2021: Future climate change shaped by inter-model differences in Atlantic Meridional Overturning Circulation response. *Nat. Commun.*, **12**, 3659, https://doi.org/10.1038/s41467-021-24015-w.

——, V. L. Meccia, R. D'Agostino, F. Fabiano, S. M. Larson, J. von Hardenberg, and S. Corti, 2023: Impacts of a weakened AMOC on precipitation over the Euro-Atlantic region in the EC-Earth3 climate model. *Climate Dyn.*, **61**, 3397–3416, https://doi.org/10.1007/s00382-023-06754-2.

Bischoff, T., and T. Schneider, 2014: Energetic constraints on the position of the intertropical convergence zone. *J. Climate*, **27**, 4937–4951, https://doi.org/10.1175/JCLI-D-13-00650.1.

Buckley, M. W., and J. Marshall, 2016: Observations, inferences, and mechanisms of the Atlantic Meridional Overturning Circulation: A review. *Rev. Geophys.*, **54**, 5–63, https://doi.org/10.1002/2015RG000493.

Byrne, M. P., and P. A. O'Gorman, 2015: The response of precipitation minus evapotranspiration to climate warming: Why the "wet-get-wetter, dry-get-drier" scaling does not hold over land. *J. Climate*, **28**, 8078–8092, https://doi.org/10.1175/JCLI-D-15-0369.1.

——, and T. Schneider, 2016: Narrowing of the ITCZ in a warming climate: Physical mechanisms. *Geophys. Res. Lett.*, **43**, 11 350–11 357, https://doi.org/10.1002/2016GL070396.

——, A. G. Pendergrass, A. D. Rapp, and K. R. Wodzicki, 2018: Response of the intertropical convergence zone to climate change: Location, width, and strength. *Curr. Climate Change Rep.*, **4**, 355–370, https://doi.org/10.1007/s40641-018-0110-5.

Broccoli, A. J., K. A. Dahl, and R. J. Stouffer, 2006: Response of the ITCZ to Northern Hemisphere cooling. *Geophys. Res. Lett.*, **33**, L01702, https://doi.org/10.1029/2005GL024546.

Caesar, L., S. Rahmstorf, A. Robinson, G. Feulner, and V. Saba, 2018: Observed fingerprint of a weakening Atlantic Ocean overturning circulation. *Nature*, **556**, 191–196, https://doi.org/10.1038/s41586-018-0006-5.

Chiang, J. C. H., and A. R. Friedman, 2012: Extratropical cooling, interhemispheric thermal gradients, and tropical climate change. *Annu. Rev. Earth Planet. Sci.*, **40**, 383–412, https://doi.org/10.1146/annurev-earth-042711-105545.

——, Y. Kushnir, and A. Giannini, 2002: Deconstructing Atlantic Intertropical Convergence Zone variability: Influence of the local cross-equatorial sea surface temperature gradient and remote forcing from the eastern equatorial Pacific. *J. Geophys. Res.*, **107**, 4004, https://doi.org/10.1029/2000JD000307.

D'Agostino, R., and P. Lionello, 2020: The atmospheric moisture budget in the Mediterranean: Mechanisms for seasonal changes in the Last Glacial Maximum and future warming scenario. *Quat. Sci. Rev.*, **241**, 106392, https://doi.org/10.1016/j.quascirev.2020.106392.

——, J. Bader, S. Bordoni, D. Ferreira, and J. Jungclaus, 2019: Northern Hemisphere monsoon response to mid-Holocene

orbital forcing and greenhouse gas-induced global warming. *Geophys. Res. Lett.*, **46**, 1591–1601, https://doi.org/10.1029/2018GL081589.

Donohoe, A., 2016: Energy and precipitation. *Nat. Geosci.*, **9**, 861–862, https://doi.org/10.1038/ngeo2846.

——, and A. Voigt, 2017: Why future shifts in tropical precipitation will likely be small. *Climate Extremes: Patterns and Mechanisms*, S.-Y. S. Wang et al., Eds., Academic Press, 115–137, https://doi.org/10.1002/9781119068020.ch8.

——, J. Marshall, D. Ferreira, and D. Mcgee, 2013: The relationship between ITCZ location and cross-equatorial atmospheric heat transport: From the seasonal cycle to the last glacial maximum. *J. Climate*, **26**, 3597–3618, https://doi.org/10.1175/JCLI-D-12-00467.1.

Eyring, V., S. Bony, G. A. Meehl, C. A. Senior, B. Stevens, R. J. Stouffer, and K. E. Taylor, 2016: Overview of the Coupled Model Intercomparison Project Phase 6 (CMIP6) experimental design and organization. *Geosci. Model Dev.*, **9**, 1937–1958, https://doi.org/10.5194/gmd-9-1937-2016.

Fernandes, K., and Coauthors, 2011: North Tropical Atlantic influence on western Amazon fire season variability. *Geophys. Res. Lett.*, **38**, L12701, https://doi.org/10.1029/2011GL047392.

Frajka-Williams, E., and Coauthors, 2019: Atlantic Meridional Overturning Circulation: Observed transport and variability. *Front. Mar. Sci.*, **6**, 260, https://doi.org/10.3389/fmars.2019.00260.

Frierson, D. M. W., and Coauthors, 2013: Contribution of ocean overturning circulation to tropical rainfall peak in the Northern Hemisphere. *Nat. Geosci.*, **6**, 940–944, https://doi.org/10.1038/ngeo1987.

Good, P., N. Boers, C. A. Boulton, J. A. Lowe, and I. Richter, 2022: How might a collapse in the Atlantic Meridional Overturning Circulation affect rainfall over tropical South America? *Climate Resilience Sustainability*, **1**, e26, https://doi.org/10.1002/cli2.26.

Held, I. M., and B. J. Soden, 2006: Robust responses of the hydrological cycle to global warming. *J. Climate*, **19**, 5686–5699, https://doi.org/10.1175/JCLI3990.1.

IPCC, 2022: *Climate Change 2022: Impacts, Adaptation and Vulnerability*. H.-O. Pörtner et al., Eds., Cambridge University Press, 3056 pp., https://doi.org/10.1017/9781009325844.

Jackson, L. C., R. Kahana, T. Graham, M. A. Ringer, T. Woollings, J. V. Mecking, and R. A. Wood, 2015: Global and European climate impacts of a slowdown of the AMOC in a high resolution GCM. *Climate Dyn.*, **45**, 3299–3316, https://doi.org/10.1007/s00382-015-2540-2.

Li, F., M. S. Lozier, N. P. Holliday, W. E. Johns, I. A. Le Bras, B. I. Moat, S. A. Cunningham, and M. F. de Jong, 2021: Observation-based estimates of heat and freshwater exchanges from the subtropical North Atlantic to the Arctic. *Prog. Oceanogr.*, **197**, 102640, https://doi.org/10.1016/j.pocean.2021.102640.

Lionello, P., R. D'Agostino, D. Ferreira, H. Nguyen, and M. S. Singh, 2024: The Hadley circulation in a changing climate. *Ann. N. Y. Acad. Sci.*, **1534**, 69–93, https://doi.org/10.1111/nyas.15114.

Liu, W., A. V. Fedorov, S.-P. Xie, and S. Hu, 2020: Climate impacts of a weakened Atlantic Meridional Overturning Circulation in a warming climate. *Sci. Adv.*, **6**, eaaz4876, https://doi.org/10.1126/sciadv.aaz4876.

Lu, J., G. A. Vecchi, and T. Reichler, 2007: Expansion of the Hadley cell under global warming. *Geophys. Res. Lett.*, **34**, L06805, https://doi.org/10.1029/2006GL028443.

Mamalakis, A., and Coauthors, 2021: Zonally contrasting shifts of the tropical rain belt in response to climate change. *Nat. Climate Change*, **11**, 143–151, https://doi.org/10.1038/s41558-020-00963-x.

Marengo, J. A., J. Tomasella, W. R. Soares, L. M. Alves, and C. A. Nobre, 2012: Extreme climatic events in the Amazon basin. *Theor. Appl. Climatol.*, **107**, 73–85, https://doi.org/10.1007/s00704-011-0465-1.

Marshall, J., A. Donohoe, D. Ferreira, and D. McGee, 2014: The ocean's role in setting the mean position of the Inter-Tropical Convergence Zone. *Climate Dyn.*, **42**, 1967–1979, https://doi.org/10.1007/s00382-013-1767-z.

McCarthy, G. D., and Coauthors, 2015: Measuring the Atlantic Meridional Overturning Circulation at 26°N. *Prog. Oceanogr.*, **130**, 91–111, https://doi.org/10.1016/j.pocean.2014.10.006.

Meccia, V. L., R. Fuentes-Franco, P. Davini, K. Bellomo, F. Fabiano, S. Yang, and J. von Hardenberg, 2023: Internal multi-centennial variability of the Atlantic Meridional Overturning Circulation simulated by EC-Earth3. *Climate Dyn.*, **60**, 3695–3712, https://doi.org/10.1007/s00382-022-06534-4.

Moreno-Chamarro, E., J. Marshall, and T. L. Delworth, 2020: Linking ITCZ migrations to the AMOC and North Atlantic/Pacific SST decadal variability. *J. Climate*, **33**, 893–905, https://doi.org/10.1175/JCLI-D-19-0258.1.

Neelin, J. D., and I. M. Held, 1987: Modeling tropical convergence based on the moist static energy budget. *Mon. Wea. Rev.*, **115**, 3–12, https://doi.org/10.1175/1520-0493(1987)115<0003:MTCBOT>2.0.CO;2.

Nicknish, P. A., J. C. H. Chiang, A. Hu, and W. R. Boos, 2023: Regional tropical rainfall shifts under global warming: An energetic perspective. *Environ. Res.: Climate*, **2**, 015007, https://doi.org/10.1088/2752-5295/acb9b0.

Nguyen, H., H. H. Hendon, E.-P. Lim, G. Boschat, E. Maloney, and B. Timbal, 2018: Variability of the extent of the Hadley circulation in the Southern Hemisphere: A regional perspective. *Climate Dyn.*, **50**, 129–142, https://doi.org/10.1007/s00382-017-3592-2.

O'Neill, B. C., and Coauthors, 2016: The Scenario Model Intercomparison Project (ScenarioMIP) for CMIP6. *Geosci. Model Dev.*, **9**, 3461–3482, https://doi.org/10.5194/gmd-9-3461-2016.

Orihuela-Pinto, B., M. H. England, and A. S. Taschetto, 2022: Interbasin and interhemispheric impacts of a collapsed Atlantic Overturning Circulation. *Nat. Climate Change*, **12**, 558–565, https://doi.org/10.1038/s41558-022-01380-y.

Parsons, L. A., J. Yin, J. T. Overpeck, R. J. Stouffer, and S. Malyshev, 2014: Influence of the Atlantic Meridional Overturning Circulation on the monsoon rainfall and carbon balance of the American tropics. *Geophys. Res. Lett.*, **41**, 146–151, https://doi.org/10.1002/2013GL058454.

Philander, S. G. H., D. Gu, G. Lambert, T. Li, D. Halpern, N.-C. Lau, and R. C. Pacanowski, 1996: Why the ITCZ is mostly north of the equator. *J. Climate*, **9**, 2958–2972, https://doi.org/10.1175/1520-0442(1996)009<2958:WTIIMN>2.0.CO;2.

Rahmstorf, S., J. E. Box, G. Feulner, M. E. Mann, A. Robinson, S. Rutherford, and E. J. Schaffernicht, 2015: Exceptional twentieth-century slowdown in Atlantic Ocean overturning circulation. *Nat. Climate Change*, **5**, 475–480, https://doi.org/10.1038/nclimate2554.

Schneider, T., T. Bischoff, and G. H. Haug, 2014: Migrations and dynamics of the intertropical convergence zone. *Nature*, **513**, 45–53, https://doi.org/10.1038/nature13636.

Schwendike, J., P. Govekar, M. J. Reeder, R. Wardle, G. J. Berry, and C. Jakob, 2014: Local partitioning of the overturning circulation in the tropics and the connection to the Hadley and

Walker circulations. *J. Geophys. Res. Atmos.*, **119**, 1322–1339, https://doi.org/10.1002/2013JD020742.

Stouffer, R. J., and Coauthors, 2006: Investigating the causes of the response of the thermohaline circulation to past and future climate changes. *J. Climate*, **19**, 1365–1387, https://doi.org/10.1175/JCLI3689.1.

Taylor, K. E., R. J. Stouffer, and G. A. Meehl, 2012: An overview of CMIP5 and the experiment design. *Bull. Amer. Meteor. Soc.*, **93**, 485–498, https://doi.org/10.1175/BAMS-D-11-00094.1.

Vellinga, M., and R. A. Wood, 2002: Global climatic impacts of a collapse of the Atlantic thermohaline circulation. *Climate Change*, **54**, 251–267, https://doi.org/10.1023/A:1016168827653.

Wang, C., L. Zhang, S.-K. Lee, L. Wu, and C. R. Mechoso, 2014: A global perspective on CMIP5 climate model biases. *Nat. Climate Change*, **4**, 201–205, https://doi.org/10.1038/nclimate2118.

Weijer, W., W. Cheng, O. A. Garuba, A. Hu, and B. T. Nadiga, 2020: CMIP6 models predict significant 21st century decline of the Atlantic Meridional Overturning Circulation. *Geophys. Res. Lett.*, **47**, e2019GL086075, https://doi.org/10.1029/2019GL086075.

Yu, S., and M. S. Pritchard, 2019: A strong role for the AMOC in partitioning global energy transport and shifting ITCZ position in response to latitudinally discrete solar forcing in CESM1.2. *J. Climate*, **32**, 2207–2226, https://doi.org/10.1175/JCLI-D-18-0360.1.

Zhang, G., and Z. Wang, 2013: Interannual variability of the Atlantic Hadley circulation in boreal summer and its impacts on tropical cyclone activity. *J. Climate*, **26**, 8529–8544, https://doi.org/10.1175/JCLI-D-12-00802.1.

Zhang, R., and T. L. Delworth, 2005: Simulated tropical response to a substantial weakening of the Atlantic thermohaline circulation. *J. Climate*, **18**, 1853–1860, https://doi.org/10.1175/JCLI3460.1.